Improvement of surface flux calculation: A study based on measurements over alpine meadow in the eastern Tibet Plateau in summer*

Li Sen(李 森) and Zhong Zhong(钟 中)†

College of Meteorology and Oceanography, PLA University of Science and Technology, Nanjing 211101, *China*

(Received 17 April 2013; revised manuscript received 28 June 2013; published online 10 December 2013)

An improved flux-gradient relationship between momentum $\varphi_{\rm m}(\zeta)$ and sensible heat $\varphi_h(\zeta)$ is obtained by the use of the observational data over an alpine meadow in the eastern Tibet Plateau, in Maqu of China during the period June to August, 2010. The empirical coefficients of Businger–Dyer type function for the cases of unstable and stable stratification are modified. Non-dimensional vertical gradients of wind and potential temperature are calculated by three fitting functions; that is, the log–linear, log–square, and log–cubic functions, respectively. It is found that the von Karman constant approaches 0.4025 and the Prandtl number is about 1.10 based on the measurements in near-neutral conditions, which are within reasonable range proposed in previous studies. The revised flux-gradient profile functions of $-1/5$ power law for momentum and $-1/3$ power law for sensible heat are best fitted in unstable stratification conditions. Meanwhile, 2/5 power law, instead of linear functions, is more appropriate in stable stratification cases for momentum and sensible heat. Compared with results from previous studies in which traditional functions are used, the momentum and sensible heat fluxes estimated by the revised profile functions in the current study are much closer to the observations for the unstable and stable stratification conditions.

Keywords: Monine–Obukhov similarity theory, flux-gradient relationship, Maqu experimental site, turbulent fluxes

PACS: 92.60.Kc, 92.60.hk, 47.27.T–, 47.27.te **DOI:** 10.1088/1674-1056/23/2/029201

1. Introduction

Turbulence exchanging process in the atmospheric boundary layer plays an important role in the atmosphere–land interaction. Accurate representations of the eddy fluxes are essential to all numerical simulations of the atmosphere.[1–3] Generally, the fluxes are either estimated with the Bowen ratio energy balance method,[4,5] or calculated by flux-profile method. The Bowen ratio method uses the difference between potential temperatures and the difference between specific humidity values at two levels, as well as the surface energy budget. But this method cannot provide the momentum flux. Furthermore, the Bowen ratio method becomes computationally unstable and results in spurious large values when the Bowen ratio is in the vicinity of -1. In the profile method, fluxes of momentum and heat in the atmospheric surface layer are estimated by non-dimensional vertical gradients of wind and temperature based on Monin–Obukhov similarity theory, and the artificial calculation with the Bowen ratio method is avoided. These gradients are usually expressed as functions of the atmospheric stability parameter z/L, where z is the measurement of height and L is the Obukhov length. However, there are many different forms and empirical constants in the formulation of the non-dimensional profile derived from *in situ* experiments. For example, based on the Kansas data over the field of wheat stubble, Businger *et al.*[6] proposed that the power law could represent the unstable stratification and log–linear relationship for stable case. However, the constants and coefficients of the flux-profile functions might not be accurate due to the significant flow distortion at the Kansas tower. New empirical coefficients were given by Dyer[7] through reviewing and revising that of Businger *et al.* Beljaars and Holtslag[8] (hereinafter B & H 1991) proposed new form of formulation for nocturnal surface after re-evaluation of the data gathered at Cabauw during the MESOGERS-84 experiment. Guilloteau[9] suggested that the scheme of Högström[10] (hereinafter H 1996) under unstable stratification and that of B & H 1991 across a wider range of stable stratification were the most accurate. But, no consensus has been reached so far on the values of the experimentally determined constants or functions. Differences in the land use and land cover type of experimental sites, duration selected for the experiments, data qualities, profile fitting methods, etc. all contribute to the discrepancies among various studies. Therefore, it is necessary and important to develop appropriate coefficients and functions according to specific surface characteristics. Great efforts have been made to achieve this goal for various underlying surface condition.[11–14]

In recent years, ecological and environmental vulnerability in the source region of the Yellow River has been inten-

*Project supported by the National Key Basic Research and Development Project of China (Grant Nos. 2011CB952002 and 2010CB428505) and the National Natural Science Foundation of China (Grant No. 41175090).

†Corresponding author. E-mail: zhong_zhong@yeah.net

© 2014 Chinese Physical Society and IOP Publishing Ltd

sified. Most areas of this region have become ecologically-environmentally fragile due to climate changes.[15] The Maqu region, one of the greatest wetlands in the Tibetan plateau, is located in the upper reach of the Yellow River. This is the major area of Yellow River runoff collection, which plays a vital role in protecting soil erosion and land desertification. It also has unique environmental and ecological characteristics, which provides an ideal location to investigate the ecological and environmental response to land surface process and climate change, and better understand water and energy budget and carbon cycle in alpine wetland ecosystem. For this reason, the Yellow River Source Region Climate and Environment Observation and Research Station (YRSRORS), affiliating to the ChinaFlux, was established in 2005.

In this study, the functional relationships between non-dimensional wind, temperature gradients, and the stability parameter are established based on the observations over Maqu of China in summer 2010. We only consider the situation where the stability parameter is within a range of $|z/L| \leq 4.0$. The rest of this paper is organized as follows. In Section 2, details of experiment and data processing are presented. In Section 3, the von Karman constant is recalculated and the profile functions of non-dimensional vertical gradients for wind and temperature are given. A comparison with previous results is made in Section 4. In Section 5, some conclusions are drawn from the present study.

2. Experiment and data

2.1. Maqu data

2.1.1. Experimental site and environment

Profiles of wind speed, air temperature and humidity, and fluxes of momentum, sensible and latent heat have been measured at the Maqu observation site. One experiment, focused on instrumental and observational practices, was carried out from November 2005 to January 2008 prior to the formal observation. The data used in this work were measured during June to August 2010. The experimental site is situated at 33°52.77′ N, 102°09.27′ E with the altitude of 3423 m, which is right in the eastern edge of the Tibetan Plateau. The terrain around this site is flat with homogeneously distributed plateau meadow. The mean height of meadow is about 20 cm (Fig. 1(a)), and the soil type consists of alpine meadow soil, alpine scrubby meadow soil, and swamp soil. The aerodynamic roughness length is about 0.035 m.[16] On the northwestern side of the site there is a mountain about 2 km far from Maqu. During the study period, the dominant wind direction was east, and other directions were distributed nonuniformly.

2.1.2. Micrometeorology measurement

A 24-m high observation tower with sensors for wind (WindSonic, Gill), temperature and relative humidity (HMP45C, Vaisala) was installed to catch aerodynamic characteristics and profiles on the surface. The observation heights are 2.35 m, 4.2 m, 7.17 m, 10.13 m, and 18.15 m above the ground (Fig. 1(b)). Accuracies of measurements are ± 0.02 ms^{-1} at 12 ms^{-1} for wind speed; ± 0.2 °C for temperature and $\pm 2\%$ at 20 °C for relative humidity. The turbulent measurements for the wind velocity components (u', v', w') and temperature (T') were acquired at a sampling rate of 10 Hz by a three-dimensional (3D) sonic anemometer/thermometer (model CSAT3, Campbell Scientific Inc., Logan, UT, USA). A data logger (model CR3000, Campbell Scientific Inc., Logan, UT, USA) recorded the eddy covariance signals for archiving and on-line computation of the turbulence statistics by eddy-covariance technique. In this study all fluxes were computed by block averaging over 30-min in the dataset, which is sufficient to capture all flux scales over a short vegetable field. In addition, an open-path CO_2/H_2O gas analyzer (model LI-7500, LI-COR, Inc., Lincoln, NE, USA) was used to measure the CO_2/H_2O fluxes.

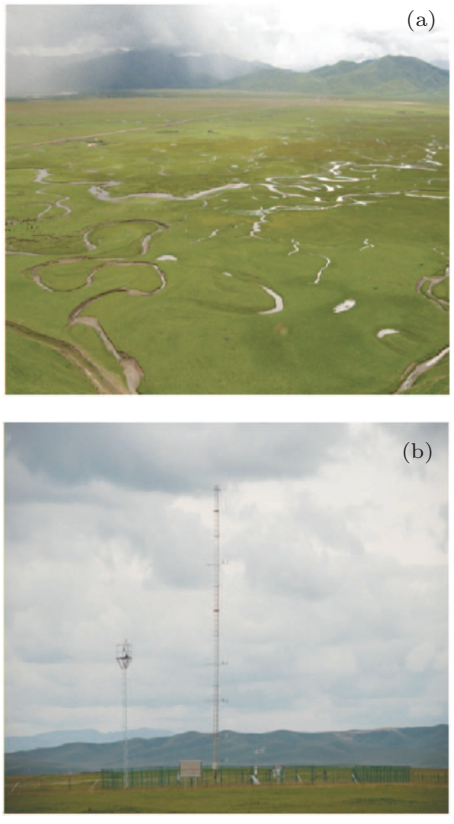


Fig. 1. (color online) The experimental site with plateau meadow (a) and the tower for fluxes and profiles measurements (b).

2.1.3. Data qualities control and selection

The hypothesis of eddy-covariance technique is that the atmospheric turbulence is in a steady state and homogeneous in the atmosphere. Hence, the steady state test and the similarity test of turbulent covariance could be used as the standard for the data quality analysis and control measured by eddy-covariance method. The flux calculations are based on the

two-rotation method to nullify the average cross-stream and vertical wind components. The planar fit method was also used for tilt correction. The WPL correction is adopted for the influences of air density variation. Sonic temperature was converted into actual temperature according to Schotanus *et al.*[17] The non-stationarity test was performed to minimize the effect of diurnal trends or weather patterns on flux computations. The fluxes data are classified into three categories as 0 (good), 1 (average), 2 (bad) according to the standard from Foken *et al.*[18] Only those best samples (category 0) were utilized in this work. More detailed description of data-processing can be found in Ref. [19] by Wang *et al.*

Due to the operation problems of the observing system, the thunderstorm weather, and the noise effects derived from environmental factors, it is necessary to exclude abnormal data, even if this will cause the loss of data. Two tests were employed in this study: the absolute limit test and the abrupt change test. The absolute limit test detected the unrealistic values in the time series. Each datum was compared with predefined minimum and maximum values: a maximum of 25 ms^{-1} for mean wind speed, -20 °C and 20 °C for mean air temperature, and 0 and 30 $\mathrm{g\cdot m}^{-3}$ for the vapor density. Since the turbulence fluxes tend to be smaller at night under stable condition, it is more difficult to carry out reliable turbulence measurements. As a result, the friction velocity was utilized as the criterion. When the friction velocity was smaller than the critical value of 0.025 ms^{-1}, the data point was regarded as being invalid. In the abrupt change test, we specified two thresholds: ± 3 times the standard deviations from the mean of the entire observed height record and from the mean of the continuous 2.5-hour measurements. When the data at a certain height or time were beyond the thresholds, the data were excluded from the analysis.

2519 flux data as well as wind and temperature profiles measured during summer (JJA) in 2010 were used in calculation. To ensure the effectiveness of the gradients-flux relationship in the following analysis, inappropriate data were excluded based on the following criteria according to Park *et al.*[12] and Song *et al.*:[13]

(i) Flux data with the absolute value of sensible heat flux (H) less than 5 $\mathrm{W\cdot m}^{-2}$ or greater than 400 $\mathrm{W\cdot m}^{-2}$, and less than -100 $\mathrm{W\cdot m}^{-2}$ in stable stratification;

(ii) Flux data with friction velocity (u_*) less than 0.025 ms^{-1} or greater than 1 ms^{-1};

(iii) Wind profiles data with mean wind speed at any height less than 1.0 ms^{-1} or the variance of wind direction at adjacent level greater than 15°;

(iv) Temperature profiles with difference at adjacent level less than 0.05 K;

(v) Given the wind speed or temperature at any height ($x_{n,z}$) in either wind or temperature profile (x_n), taking 3 times the standard deviation

$$\sigma_n = \left(\frac{1}{5}\sum_{k=1}^{5}(x_{n,k}-\overline{x_n})^2\right)^{1/2}$$

from profile data as the threshold, where $\bar{x}_n$ is the mean value of x_n, if $x_{n,z}$ lay beyond the range $[\overline{x_n}-3\sigma_n, \overline{x_n}+3\sigma_n]$, the profile was rejected.

(vi) Badly fitted profiles with large fitting errors (FE), which is defined as the ratio of the root mean square error of the fitting to the range of value in the profile, i.e.,

$$\mathrm{FE} = \frac{\left(\frac{1}{5}\sum_{k=1}^{5}\left(x'_{n,k}-x_{n,k}\right)^2\right)^{1/2}}{\max\left(x_{n,k}\right)-\min\left(x_{n,k}\right)},$$

where $x'_{n,k}$ is the fitted value with LCF fitting function relative to $x_{n,h}$.

Through the above quality control and criteria screening, 1590 wind profiles, of which 1118 are for unstable stratification and 472 are for stable stratification, as well as fluxes data at the same moment were obtained for the determination of non-dimensional wind vertical gradient and monument flux relationship; whereas 789 temperature profiles, of which 571 are for unstable stratification and 218 are for stable stratification, and simultaneous flux data were obtained for the non-dimensional temperature vertical gradient and the sensible heat flux relationship.

2.2. SACOL data

To examine the validity of the new flux-profile functions based on Maqu data, the data provided by Semi-Arid Climate and Environment Observatory in Lanzhou University (SACOL), which was established in 2005, are used for comparison.

2.2.1. Experimental site and environment

SACOL, situated at the semi-arid site of China-Loess Plateau, about 1965.8 m above sea level, is on the southern bank of the Yellow River in Gansu province Northwestern China (35.57° N, 104.08° E), about 48 km away from the city of Lanzhou. The site is located on a nearly north–south mesa in the most common wind direction. The terrain where the measurements were carried out is flat and covered mainly with short grass that is usually less than 15 cm tall. SACOL consists of a large set of instruments and measurements; for example, boundary layer meteorological parameters, surface radiation, surface fluxes, soil heat and water moisture, ambient air quality, aerosol optical, temperature and water vapor profiles, sky conditions, etc.

2.2.2. Measurements

In the work, boundary layer meteorological parameters and surface fluxes data collected in SACOL are used. Wind

speeds (014A-L, Met One), air temperatures and relative humidity values (HMP45C-L, Vaisalla) at 1, 2, 4, 8, 12, 16, and 32 m, and wind direction (034B-L, Met One) at 8 m, with signals logged to a data logger (CR23X, Campbell), are recorded with half-hour intervals. The skin temperature and air pressure are measured using a Precision Infrared Thermocouple Sensor (IRTS-P, Apogee) and a CS105 Barometric Pressure Sensor (Vaisala). The surface fluxes of momentum, CO_2, sensible and latent are measured through eddy covariance system with a three-axis Sonic Anemometer (CSAT3, Campbell) and an opened path infrared CO_2 and H_2O analyzer (LI7500, LI_COR). These eddy covariance signals are logged to a data logger (CR5000, Campbell) at 10 Hz and then all fluxes were also computed for averaging 30-min. Details of SACOL can be found in Ref. [20] by Huang *et al.* and Ref. [21] by Wang *et al.*

2.2.3. Data quality controls

To obtain the turbulent flux data accurately, the quality controls are necessary. All the procedures for corrections and quality controls are adopted:[22] coordinating rotation using the planar fit method, sonic temperature correction, WPL correction (correction for density fluctuations), time delay correction, frequency response correction, and integral turbulent characteristics (ITC) test under the turbulence development condition for the vertical velocity. Through the post-field data processing, the SACOL data could be considered as reliable inspection data. The period from August 1 to 15, 2008 was selected to conduct the profile measurements and turbulence measurements for this study with a total of 580 samples.

3. Results

Based on the similarity hypothesis of Monin and Obukhov, the non-dimensional wind and potential temperature profile functions in a horizontally homogeneous surface layer are expressed as follows.

For momentum

$$\varphi_{\mathrm{m}}(\zeta) = \frac{\kappa z}{u_*}\frac{\partial \overline{u}}{\partial z}, \tag{1}$$

and for sensible heat flux

$$\varphi_{\mathrm{h}}(\zeta) = \frac{\kappa z}{\theta_*}\frac{\partial \overline{\theta}}{\partial z}, \tag{2}$$

where $\overline{u}$ is the mean horizontal wind speed, $\overline{\theta}$ is the potential temperature, u_* is the friction velocity, θ_* is the temperature scaling, κ is the von Karman constant, $\zeta = z/L$ is the stability parameter, and L is the Obukhov length given by $L = \overline{\theta}u_*^2/\kappa g\theta_*$. In this study, on the basis of Businger–Dyer type profile functions,[6,7] improved flux-gradient relationships suitable for Maqu are developed by using the above selected data.

3.1. Calculations of vertical gradients

Due to the limited height in observation and possible systematic bias caused by using large interval in differential calculation, the fitting function method is adopted in this study for vertical gradient calculations. The vertical profiles of wind and temperature are fitted by three fitting functions;[12] that is, the log–linear function (LLF), log–square function (LSF), and log–cubic function (LCF). They are given below.

$$\begin{aligned} x(z)_{\mathrm{LLF}} &= c_1 + c_2 \ln z + c_3 z, \\ x(z)_{\mathrm{LSF}} &= c_1 + c_2 \ln z + c_3 (\ln z)^2, \\ x(z)_{\mathrm{LCF}} &= c_1 + c_2 \ln z + c_3 (\ln z)^2 + c_4 (\ln z)^3, \end{aligned} \tag{3}$$

where $x(z)$ is the fitted value of wind speed or temperature at the height of z, and c_1–c_4 are the constant coefficients. After determining the coefficients using the observation data, the mean vertical gradients at a given height could be calculated through derivatives of the expressions. At the same height, the differences between calculated gradients result from different functions. However, for both wind and potential temperature, the sensitivities of computed gradients to three fitting functions vary with height adopted. As shown in Figs. 2 and 3, at the level of 4.2 m, small differences among the three fitting functions are obtained. This result indicates that the gradients are not sensitive to the selected function. On the contrary,

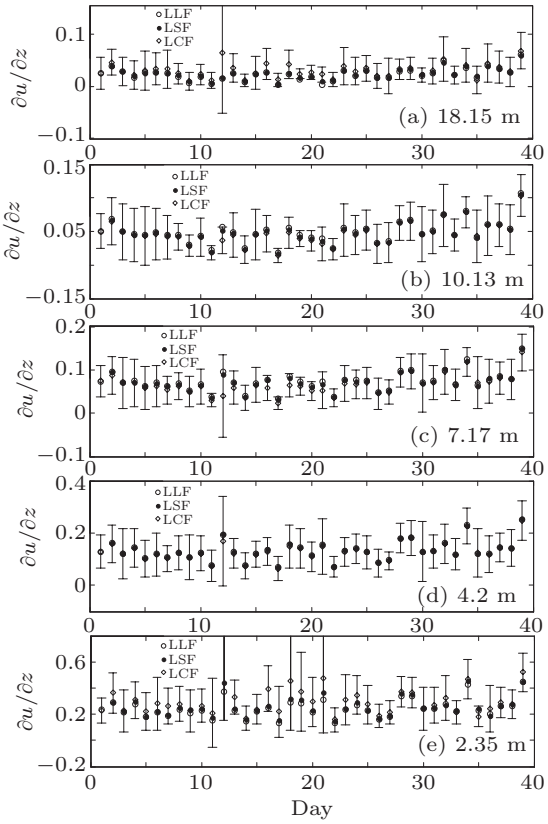


Fig. 2. Daily variations of the wind vertical gradients at 2.35 m, 4.2 m, 7.17 m, 10.13 m, and 18.15 m with day in a period from 1st June to 5th July 2010. The error bar represents the standard deviation of gradients calculated by LCF function.

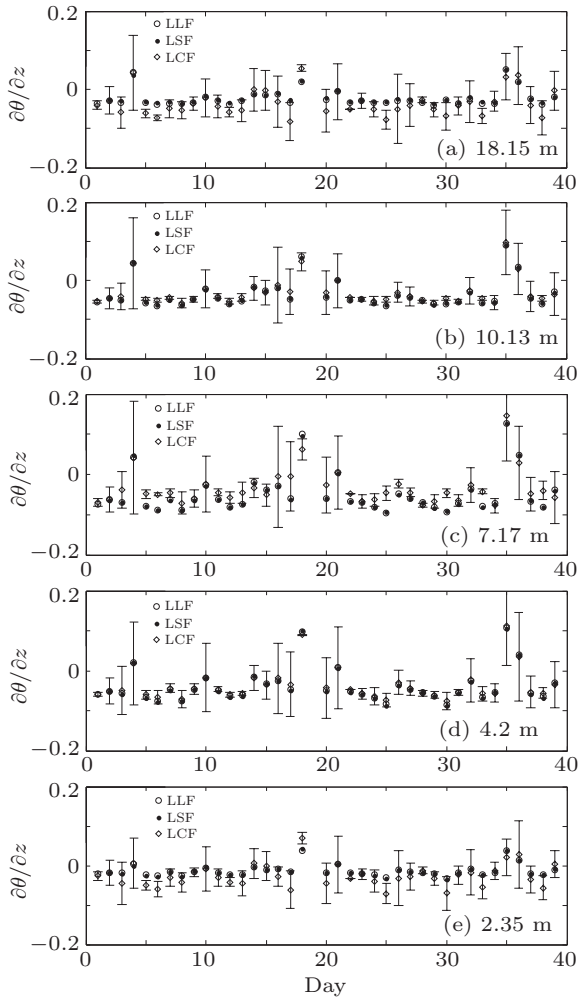


Fig. 3. The same as Fig. 2, but for vertical gradient of potential temperature.

at levels lower than 4.2 m or at the highest level of 18.15 m, greater differences appear and may lead to inconsistency in the gradient calculation. To reduce the uncertainty caused by different functions in gradient calculation, the lowest sensitive height of 4.2 m for gradient calculation is adopted.

3.2. Issue of Von Karman constant κ

It has been generally recognized that the von Karman constant κ may be a major cause for the discrepancy between flux calculations with various analytical expressions for φ_m and φ_h. Its values in various experiments are different, varying in a range from 0.35 to 0.42.[23] There are few papers in available literature to explain the reason of the difference. So, the accurate value of κ is still an issue in argument. In this paper, κ is assumed to be constant and computed directly with data in neutral stratification case ($\zeta = 0$), where φ_m is unity by definition. Then, equation (1) can be simplified into

$$\frac{1}{\kappa} = \frac{z}{u_*}\frac{\partial \overline{u}}{\partial z}, \quad \text{at} \quad \zeta = 0. \tag{4}$$

The neutral stratification, in which stress and buoyancy effect are small, usually occurs in cloudy and windy days with large uncertainty. Therefore, the data in typical neutral condition are not easily obtained. Here, we assume that $|\zeta| \le 0.01$ would indicate the neutral stratification, and κ is considered to be equal to the mean value of $(z/u_* \cdot \partial\overline{u}/\partial z)^{-1}$ for this range. Figure 4 shows the scatter plot of $(z/u_* \cdot \partial\overline{u}/\partial z)^{-1}$ against $|\zeta|$ for neutral stratification using three fitting methods with the values of averaging κ of 0.4003, 0.3968, and 0.4104 from 34 samples. The von Karman constant of 0.4025 is obtained by averaging the values from three fitting methods, which is reasonable from the point of view of previous studies and compared with the traditionally used value of 0.4.

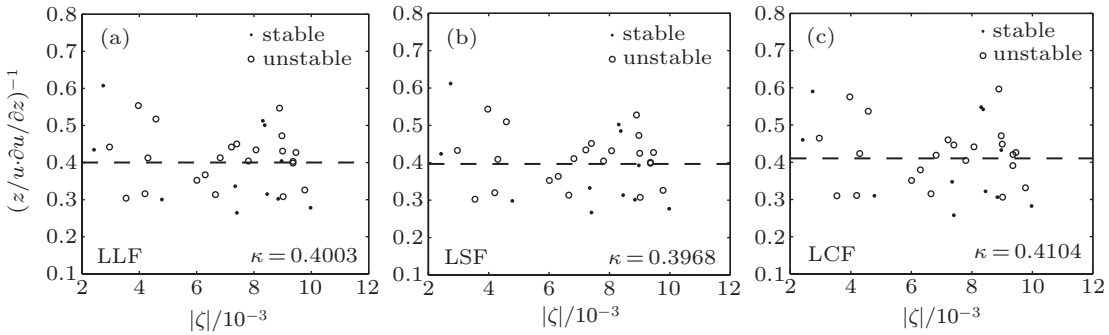


Fig. 4. Plots of $(z/u_z \cdot \partial\overline{u}/\partial z)$ against $|\zeta|$ in a range of $|\zeta| \le 0.01$ for neutral stratification with three fitting methods (the dashed line shows mean value among 34 samples) (a): LLF, (b): LSF, (c): LCF.

3.3. Non-dimensional wind and temperature profiles functions φ_m and φ_h

So far, Businger–Dyer type profile function given by Eq. (5) for the unstable case is assumed to be satisfactory and acceptable in general. However, quite different coefficients of the universal function are obtained from previous studies. In the current study, the following form of equation is used for both unstable conditions and stable stratification:

$$\varphi_x = a_x\left(1 + b_x\frac{z}{L}\right)^{c_x}, \tag{5}$$

where x represents the momentum (m) or sensible heat (h), a_x, b_x, and c_x are the empirical coefficients to be computed.

Using the flux and gradient data, the calculation process for those coefficients are introduced below.

First, in Eq. (5), a_x is determined in near-neutral stratification where $|\zeta| \leq 0.02$. As shown in Fig. 5, a_x is considered to be equal to φ_x at $\zeta = 0$, which is in consistence with the intercept of linear regression function between φ_x and ζ in the range mentioned above, with the values of 1.0484, 1.0565, and 1.026, averaged to be 1.0437 for momentum and of 1.1629, 1.2006, and 1.1106, averaged to be 1.1580 for sensible heat, respectively.

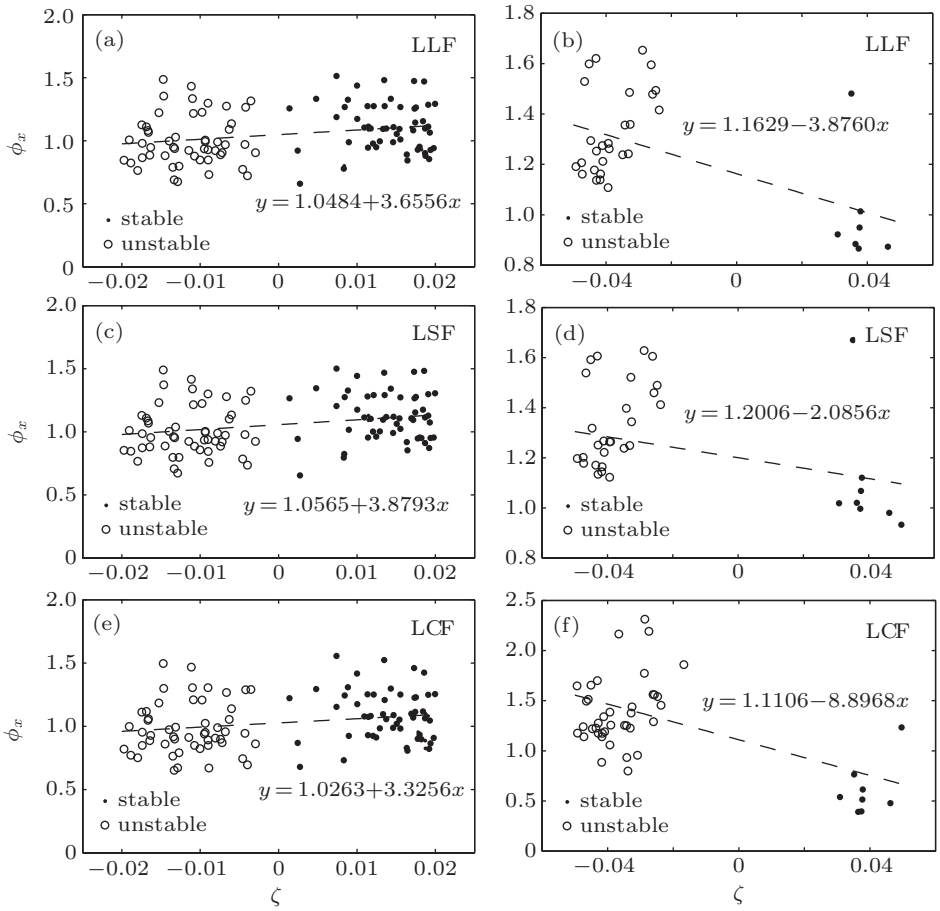


Fig. 5. Determinations of a_x in near-neutral conditions for three fitting methods (the reference line is the linear fitting curve of scatter plot in each panel), (a), (c), (e): momentum, (b), (d), (f): sensible heat.

Second, b_x was assumed to be 10 as an initial guess value in this paper before calculation. This assumption is adopted because b_x is assumed to be the constant on the order of 10 in most of earlier studies. The logarithm of Eq. (5) could then be expressed as

$$\ln \varphi_x = c_x \ln \frac{10z}{L} + \ln a_x, \tag{6}$$

where c_x is converted into the slope of the expression and yielded from selected data at the height of 4.2 m by three fitting methods, and its values are -0.2189, -0.2108, and -0.2185 for momentum and -0.2892, -0.2837, and -0.3046 for sensible heat in unstable stratification (Fig. 6), while in stable stratification its values are 0.3776, 0.3703, and 0.3922 for momentum and 0.3968, 0.3615, and 0.4421 for sensible heat (not shown). Note that through the above process, values of c_x are consistently good for three fitting methods. For simplicity, by approaching to the mean fitted value among fitting methods, c_x is identified as $-1/5$ for momentum and $-1/3$ for sensible heat in unstable stratification. These values are somewhat smaller than that of Businger *et al.*[4] In the stable stratification, instead of the log–linear relationship, the values of c_x for momentum and sensible heat are both taken to be 2/5.

Third, after a_x and c_x are obtained, b_x could be determined through Eq. (5) by the least square regression. Based on all the φ_x values calculated by Eqs. (2) and (3), the values of b_x are determined to be -33.9471 and 36.4718 for momentum and -8.9053 and 59.4843 for sensible heat in unstable and stable stratification, respectively.

Finally, the profile functions for $\varphi_{\mathrm{m}}(\zeta)$ and $\varphi_{\mathrm{h}}(\zeta)$ are

given as Eqs. (7) and (8). For unstable stratification ($\zeta < 0$)

$$\varphi_{\rm m}(\zeta) = 1.0437(1-33.9\zeta)^{-1/5}, \tag{7a}$$

$$\varphi_{\rm h}(\zeta) = 1.1580(1-8.9\zeta)^{-1/3}, \tag{7b}$$

and for stable stratification ($\zeta > 0$)

$$\varphi_{\rm m}(\zeta) = 1.0437(1+36.5\zeta)^{2/5}, \tag{8a}$$

$$\varphi_{\rm h}(\zeta) = 1.1580(1+59.5\zeta)^{2/5}. \tag{8b}$$

The Prandtl number, which is a dimensionless number defined as the ratio of the eddy diffusivity for heat to momentum, that is, $\mathrm{Pr}_t = \varphi_{\rm h}(\zeta)/\varphi_{\rm m}(\zeta)$, Pr_t is 1.10 for near-neutral conditions, which is in a range of the results given by Schumann and Gerz (1995).[24]

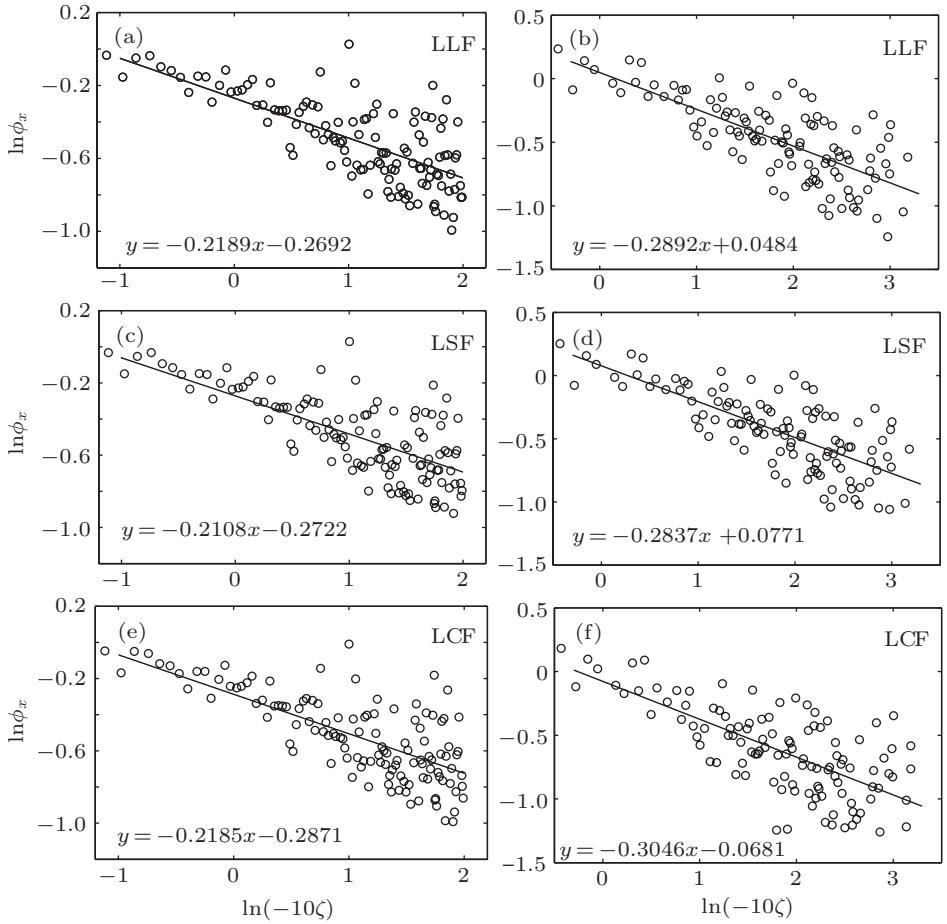


Fig. 6. Determinations of c_x in unstable conditions ($-3 < \zeta < 0$) for three fitting methods (the solid line represents the least-squares fit through the data points in each panel), (a), (c), (e): momentum, (b), (d), (f): sensible heat.

4. Preliminary verification

4.1. Flux-profile relationships

To examine the validity of the obtained $\varphi_{\rm m}(\zeta)$ and $\varphi_{\rm h}(\zeta)$, we compare them with other empirical formulations in previous studies using the selected SACOL data. The profile functions of the atmospheric stability parameter, such as Businger *et al.*,[6] Dyer,[7] Wieringa,[25] Cheng and Brutsaert[26] (hereinafter C & B 2005) for stable stratification, H 1996 for unstable stratification, and B & H 1991 for stable stratification, are taken as references. The comparisons are conducted by calculating $\varphi_{\rm m}(\zeta)$ and $\varphi_{\rm h}(\zeta)$ from different references. As shown in Fig. 7(a), in unstable stratification ($-5 < \zeta < 0$), the fitted $\varphi_{\rm m}(\zeta)$ values among the functions are consistent with each other, and the general trend of the scatter can be well represented. However, it can be seen that the discrepancy among different schemes increases with the increase of ζ. In the weak stable condition ($0 < \zeta < 0.5$), the log–linear functions performed better, as indicated by Businger *et al.*[6] and Dyer,[7] but the same functions severely overestimated the values when $\zeta > 0.4$. If $\varphi_{\rm m}(\zeta)$ is overestimated, then u_* is underestimated and so are the momentum fluxes. It is clear that with all the C & B 2005, B & H 1991 and newly scheme, the growth rate of calculated $\varphi_{\rm m}(\zeta)$ decreases as ζ increases, which is in agreement with the measurements. However, our new scheme matches well the measurements in magnitude compared with the others. On the other hand, as shown in Fig. 7(b), the values of $\varphi_{\rm h}(\zeta)$ obtained by references are underestimated com-

pared with observation, and this underestimation is gradually evident in a range of $\zeta < 1$. Note that the values of $\varphi_h(\zeta)$ calculated by C & B 2005 and our scheme accord well with each other within $0 < \zeta < 1$, but the underestimation in the growth rate of $\varphi_h(\zeta)$ computed by C & B 2005 is obvious. Although little difference is found between B & H 1991 and our new scheme when $1.5 < \zeta < 3.5$, the underestimation should not be ignored in $0 < \zeta < 1.2$. In order to further assess the match of results by those functions with measurements, the normalized standard error of the estimation (NSEE) can be calculated from

$$\mathrm{NSEE} = \sqrt{\frac{\sum_{i=1}^{n}(L_i - C_i)^2}{\sum_{i=1}^{n}(C_i)^2}}, \tag{9}$$

where L_i represents the results obtained from different empirical functions, C_i values are the corresponding results calculated by Eqs. (2) and (3), and n represents the number of data in each stability bin. It can be seen from Table 1 that, over the entire stability range, new functions perform higher fitting accuracy and lower dispersion than others, while the H 1996 for an unstable case and B & H 1991 for a stable case.

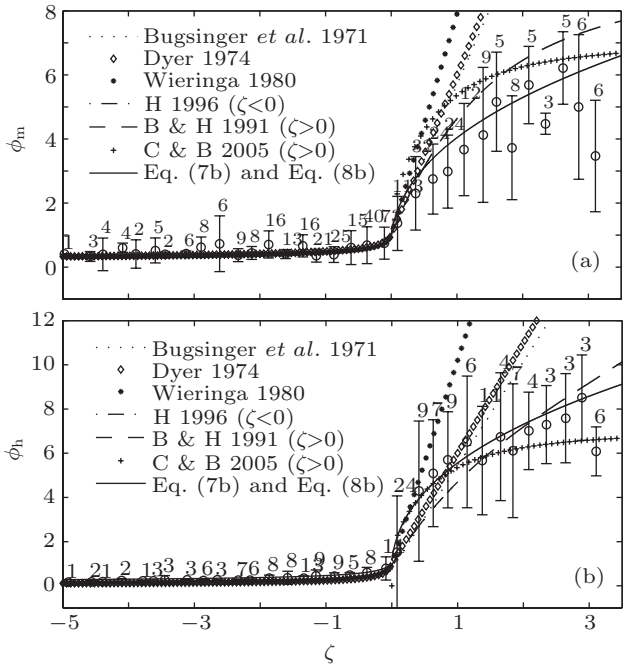


Fig. 7. Flux-gradient relationships of (a) wind and (b) potential temperature with ζ. The circles represent the mean value measured by Eq. (2) and Eq. (3) with selected data. Error bars indicate the standard deviation of the individual results contributing to the mean value. The number of samples in each stability bin of $\Delta\zeta = 0.15$ is shown above the error bar.

Table 1. Normalized standard errors of the estimation (NSEE) of $\varphi_x(\zeta)$ for momentum and sensible heat flux to the measurements calculated by different empirical functions of Businger *et al.*, Dyer, Wieringa, H 1996, B & H 1991, C & B 2005, and Eq. (7) and Eq. (8).

		Businger *et al.* 1971	Dyer 1974	Wieringa 1980	B & H 1991	H 1996	C & B 2005	Eq. (7) and Eq. (8)
Unstable	$\varphi_m(\xi)$	0.5730	0.5737	0.5791		0.5732		0.5625
	$\varphi_h(\xi)$	0.5917	0.5861	0.5605		0.5564		0.5370
Stable	$\varphi_m(\xi)$	1.2582	1.3575	2.0088	0.6142		0.6857	0.5344
	$\varphi_h(\xi)$	1.1093	0.8076	1.8496	0.4482		0.4503	0.4111

4.2. Flux estimations

To determine whether the new gradient-flux relationship is suitable for estimating fluxes, it is desirable to calculate fluxes with it and compare them with direct measurements. For this purpose, the scheme of H 1996 for the unstable stratification and B & H 1991 for the stable stratification are used in our comparison. The differences between the new scheme and the references are significant, which would help illustrate the superiority of the new scheme. Integrating Eqs. (1) and (2) with respect to z, we can obtain

$$u_* = u(z)\kappa\left[\ln\frac{z}{z_{0m}} - \psi_m\left(\frac{z}{L}\right) + \psi_m\left(\frac{z_{0m}}{L}\right)\right]^{-1}, \tag{10a}$$

$$\theta_* = [\theta(z) - \theta(z_{0h})]\,\kappa\left[\ln\frac{z}{z_{0h}} - \psi_h\left(\frac{z}{L}\right) + \psi_h\left(\frac{z_{0h}}{L}\right)\right]^{-1}, \tag{10b}$$

where z_{0m} and z_{0h} are the roughness lengths for momentum and heat, with $z_{0m} = 0.035$ m and $z_{0h} = 0.1 z_{0m}$; $\psi_m(z/L)$ and $\psi_h(z/L)$ are the stability functions obtained by integrating Eqs. (7) and (8) with respect to ζ, and the results are expressed as Eq. (11) and (12):

$$\psi_m\left(\frac{z}{L}\right) = 0.7\ln\left(x^2 - 0.62x + 1\right) - 0.9\arctan\frac{4x - 1.24}{3.8} + 1.8\ln\left(x^2 + 1.62x + 1\right) - 1.8\arctan\frac{4x + 3.24}{2.4} + 0.1282, \tag{11a}$$

$$\psi_h\left(\frac{z}{L}\right) = \ln\left(y^3 - 1\right) - 1.158\ln(y - 1) + 0.58\ln\left(y^2 + y + 1\right) - 2\arctan\frac{2y + 1}{1.73} + 0.3657, \tag{11b}$$

for unstable condition ($\zeta < 0$), where $x = (1 - \gamma_m z/L)^{1/5}$, $y = (1 - \gamma_h z/L)^{1/3}$, $\gamma_m = 33.9$, $\gamma_h = 8.9$; and

$$\psi_m\left(\frac{z}{L}\right) = \ln\left|\frac{x^5 - 1}{x - 1}\right| - 2.5x^2 + 0.8\ln\left(x^2 - 0.62x + 1\right) + 1.18\arctan\frac{4x - 1.24}{3.8} - 0.31\ln\left(x^2 + 1.62x + 1\right) - 1.9\arctan\frac{4x + 3.24}{2.4} + 2.6539, \tag{12a}$$

$$\psi_{\rm h}\left(\frac{z}{L}\right) = \ln\left|\frac{y^5-1}{(y-1)^{1.158}}\right| - 2.9y^2 + 0.93\ln\left(y^2-0.62y+1\right) + 1.37\arctan\frac{4y-1.24}{3.8} - 0.36\ln\left(y^2+1.62y+1\right) - 2.2\arctan\frac{4y+3.24}{2.4} + 3.3275, \quad (12b)$$

for stable condition ($\zeta > 0$), where $x = (1+\gamma_{\rm m} z/L)^{1/5}$, $y = (1+\gamma_{\rm h} z/L)^{1/5}$, $\gamma_{\rm m} = 36.5$, and $\gamma_{\rm h} = 59.5$.

Figure 8(a) shows the comparisons among the momentum fluxes ($\tau = \rho u_*^2$) measured by the sonic anemometer, those of H 1996 for unstable conditions and B & H 1991 for stable conditions, and the results of our new method for the SACOL data measured during August 1 to 15, 2008. These comparisons could be considered as an isolated test for different schemes. It can be seen that the estimations of τ by Eqs. (10a), (11a), and (12a) are much more consistent with the observations than those by H 1996. Apparently, our new scheme greatly reduces the overestimation by H 1996. It should be noted that the momentum fluxes with new scheme are almost identical to that with B & H 1991 in $0 < z/L < 1.3$, where reliable functions are available.[21] Moreover, the improvement for momentum fluxes by present scheme against B & H 1991 becomes clearer as ζ increases for stable cases. Although the improvement is not the same significant under weak stable condition, the difference between observed τ and estimated one by our new scheme is close to zero in strong stable cases (Fig. 8(b)). In the unstable stratification, the mean relative error is less than 41%, and reduced by 18.22% compared with that of H 1996. The absolute error decreases to about 1/3 of that of H 1996. In contrast with B & H 1991 schemes for stable cases, the relative error decreases by 20%.

More comparisons are conducted in this study to investigate the ability for our new scheme to predict the sensible heat fluxes. It could be seen that the computed sensible heat fluxes with new functions are somewhat less than the measurements in most stratifications. Nevertheless, the fluxes calculated by H 1996 are greater than the measurements evidently, and the obvious underestimations computed by B & H 1991 are found (Fig. 9(a)). It is clear that under both stable and unstable situation, our new scheme performs better than the other two schemes used here since a lager value of $\varphi_{\rm h}$ is determined. As a result, the relative error decreases by 8.42% compared with that of H 1996 for unstable cases, and 13.03% with respect to that of B & H 1991 for stable cases (Fig. 9(b)). However, despite the fact that there is no serious discrepancy between $H_{\rm s}$ calculated by our new scheme and the measured one, the improvement is not so significant as that of τ due to the fact that the value of $z_{0\rm h}$ is determined empirically.

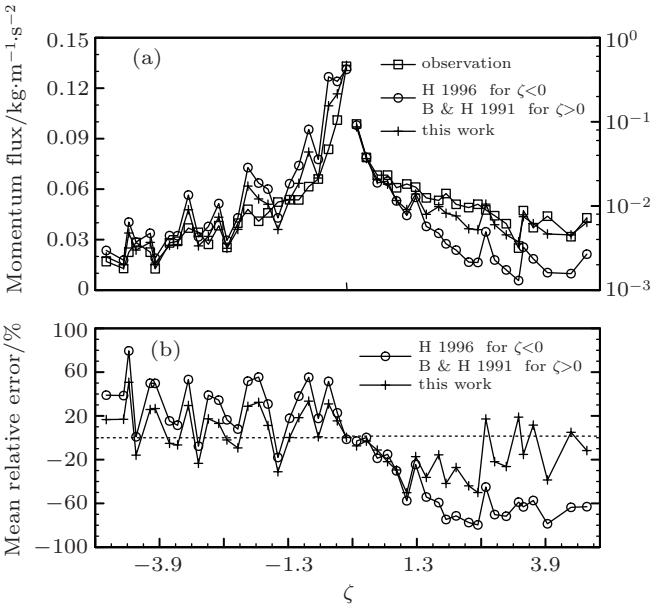


Fig. 8. (a) Momentum fluxes measured by the sonic anemometer (square) and estimated by the H 1996 for unstable scheme, B & H 1991 for stable stratification scheme (circle), and proposed scheme in this paper (cross). The left y axis indicates the unstable cases, the right for stable cases. (b) The mean relative error of momentum fluxes between the observations and estimation schemes.

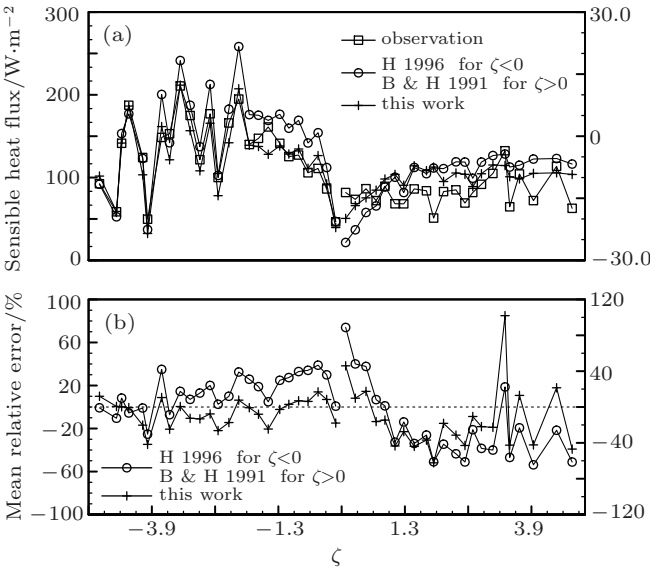


Fig. 9. The same as Fig. 8, but for the sensible heat fluxes.

In general, according to the comparison between the mean relative errors, it is indicated clearly that our new functions in this study perform better and have a more accurate prediction for momentum and sensible heat fluxes than other reference empirical functions.

5. Conclusions

The flux-gradient relationships of momentum and sensible heat are analyzed through curvilinear regression from YRSRORS in summer over Maqu of China, which is char-

acterized by flat terrain that is homogeneously covered with plateau meadow.

It is found that $\kappa = 0.4025$ coincides with previous result for this experiment, based on data in a range of $|\zeta| \leq 0.01$ as the neutral stratification. Furthermore, by analyzing our data in near-neutral condition, the Prandtl number is determined to be 1.10, but larger than the 'classical' value of unity or 0.74.[4]

The non-dimensional profile functions are obtained using high-quality fluxes and micrometeorology measurements. Coefficients of Businger–Dyer form functions in a range of $|z/L| \leq 4.0$ are revised to obtain more realistic results. Analyses in the unstable stratification for momentum and sensible heat show that $-1/5$ power law and $-1/3$ power law seem to be more appropriate from optimal regression in this study. Compared with the 'classical' $-1/4$ and $-1/2$ power laws used by H 1996, results from our new profile functions greatly reduce the relative error of estimated momentum and sensible heat fluxes from SACOL by 18.22% and 8.42%, respectively. In the stable stratification, power-type functions are also taken instead of 'traditional' log–linear functions. For both momentum and sensible heat, 2/5 power law is suggested by curvilinear regression, which evidently accords better with observation than the case of linear empirical functions. Furthermore, the relative errors of computed momentum fluxes and the sensible heat decrease by 20% and 13.03% respectively compared with that of B & H 1991 scheme, which is used widely. However, the comparisons also indicate that improvement of the estimated sensible heat fluxes is not so significant as that of the estimated momentum fluxes.

The application of the flux-gradient relationships presented in this paper in numerical models is still under investigation. The analytical solutions could be solved by substituting the new flux-gradient functions into the Monin–Obukhov stability parameter equation, and it may be imposed into the model to simulate the energy exchange accurately in the source region of Yellow River.

Acknowledgment

We wish to thank Dr. Zhang Yu of Cold and Arid Regions Environmental and Engineering Research Institute, Chinese Academy of Sciences, for providing the observational data of the Yellow River Source Region Climate and Environment Observation and Research Station in Maqu and also for SACOL.

References

[1] Kalma J D, Franks S W and Van den Hurk B J J M 2001 *Meteorol. Atmosph. Phys.* **76** 53
[2] Dai X G, Wang P and Zhang K J 2012 *Chin. Phys. B* **21** 119201
[3] Ran L K, Yang W X and Chu Y L 2010 *Chin. Phys.* B **19** 079102
[4] Fritschen L J and Simpson J R 1989 *J. Appl. Meteorol.* **28** 680
[5] Wu H and Shen S 2000 *J. Atmosph. Sci.* **20** 537 (in Chinese)
[6] Businger J A, Wyngaard J C, Izumi Y and Bradley E F 1971 *J. Atmosph. Sci.* **28** 181
[7] Dyer A J 1974 *Bound. Layer Meteorol.* **7** 363
[8] Beljaars A C M and Holtslag A A M 1991 *J. Appl. Meteorol.* **30** 327
[9] Guilloteau E 1998 *Bound. Layer Meteorol.* **87** 147
[10] Högström U 1996 *Bound. Layer Meteorol.* **78** 215
[11] Zhao M 2000 *J. Atmosph. Sci.* **20** 317 (in Chinese)
[12] Park S J, Park S U, Ho C H and Mahrt L 2009 *J. Geophys. Res.* **114** D08115
[13] Song X, Zhang H, Chen J and Park S 2010 *Bound. Layer Meteorol.* **134** 487
[14] Zhang G, Leclerc M Y and Karipot A 2010 *Biogeosci. Discuss.* **7** 4505
[15] Yang J, Ding Y and Chen R 2007 *J. Desert Res.* **27** 1012 (in Chinese)
[16] Li S, Lü S, Liu Y, Zhang Y, Ao Y, Gao Y, Cheng S and Shang L 2006 *Plateau. Meteorol.* **29** 1408 (in Chinese)
[17] Schotanus P, Nieuwstadt F and Bruin H 1983 *Bound. Layer Meteorol.* **26** 81
[18] Foken T, Gockede M, Mauder M, Mahrt L, Amiro B and Munger W 2004 *"Post-Filed Data Quality Control"*, (ed.) Law, in *Handbook of Micrometeorology: A Guide for Surface Flux Measurement and Analysis*, eds. Lee X and Massman W B (Dordrecht: Kluwer Academic Publisher) p. 181
[19] Wang S Y, Zhang Y, Lü S H, Liu H P and Shang L Y 2013 *Adv. Atmos. Sci.* **30** 411
[20] Huang J P, Zhang W, Zuo J Q, Bi J R, Shi J S, Wang X, Chang Z L, Huang Z W, Yang S, Zhang B D, Wang G Y, Fang G H, Yuan J Y, Zhang L, Zuo H C, Wang S G, Fu C B and Chou J F 2008 *Adv. Atmos. Sci.* **25** 906
[21] Wang G Y, Huang J P, Guo W D, Zuo J Q, Wang J M, Bi R J, Huang Z W and Shi J S 2010 *J. Geophys. Res.* **115** D00K17
[22] Zuo J Q, Huang J P, Wang J M, Zhang W, Bi R J, Wang G Y, Li W J and Fu P J 2009 *Adv. Atmos. Sci.* **26** 679
[23] Andreas E L 2009 *J. Appl. Meteorol. Climatol.* **48** 923
[24] Schumann U and Gerz T 1995 *J. Appl. Meteorol.* **34** 33
[25] Wieringa J 1980 *Bound Layer Meteorl.* **18** 411
[26] Cheng Y and Brutsaert W 2005 *Bound Layer Meteorol.* **114** 519